Rare Metal Materials and Engineering
Volume 47, Issue 12, December 2018
Online English edition of the Chinese language journal

Available online at www.sciencedirect.com
ScienceDirect

Cite this article as: Rare Metal Materials and Engineering, 2018, 47(12): 3672-3677.

ARTICLE

Oxygenated Treatment on Saturated Vapour Oxidation Behaviors of GH2984 Alloys for 700 °C Ultra-supercritical Boilers

Wang Yu[1], Liu Jiangnan[1], Wang Zhengpin[1], Yao Yuhong[1], Yu Zaisong[2], Lu Jintao[2]

[1] Xi'an Technological University, Xi'an 710021, China; [2] Xi'an Thermal Power Research Institute Co. Ltd, Xi'an 710032, China

Abstract: The saturated vapor oxidation behavior of GH2984 alloys at 750 °C were investigated by oxidation weight increasing method, X-ray diffraction and scanning electronic microscopy in different dissolved oxygen concentrations. The results show that the oxide film of GH2984 alloys in different dissolved oxygen concentrations is of a single layer consisting of continuous Cr_2O_3. The oxidation mass gain of GH2984 alloys slightly increases with the increase of the dissolved oxygen concentrations in water vapor. Oxygenated treatment could accelerate the internal oxidation phenomenon, enhance the oxidation film thickness and make the scattered nodular bulges of Fe_2O_3 disappear and more Cr-rich nodular bulges form. Moreover, high dissolved oxygen concentrations do not affect the stabilization of Cr_2O_3 but contribute to the formation of a little Al_2O_3 and TiO_2 which are oxidized internally.

Key words: GH2984 alloys; vapour oxidation; oxygenated treatment; oxidation film

For reducing environmental pollutions and improving coal energy efficiency, since the end of the 20th century the ultra-supercritical units have sequentially been developed in many countries around the world. Thermal AD700 Power Plant was launched in Europe at the end of 20th century to build 37.5 MPa/700 °C/720 °C ultra-supercritical demonstration power station[1]. United States have begun to develop the ultra-supercritical unit with the supercritical steam parameter of 38 MPa/760 °C/760 °C[2]. Japan has also started to build 35 MPa/700 °C/720 °C ultra-supercritical thermal power units[3]. China launched the national project of the key technology, equipment development and application model for 700 °C ultra-supercritical coal-fired power generation in 2011. However, it was greatly restricted by the properties of high-temperature materials. The maximum service temperature of austenitic stainless steel used in the superheater and reheater was only 675 °C with serious oxidation and it could not meet the requirements of 700 °C ultra-supercritical units. So nickel- base and nickel iron-base alloys, like Inconel 740H and GH2984, were attracting widespread interest to be used in the superheater and reheater of 700 °C ultra-supercritical units[4]. GH2984 was a Fe-Ni base high-temperature alloy with better high temperature mechanical properties developed by the Institute of Metal Research (IMR), Chinese Academy of Sciences (CAS)[5]. 700 °C tensile strength of GH2984 was slightly less than that of Inconel 740H and 700 °C endurance strengths for 30 000 and 100 000 h were in the same level as Inconel 740H.

It has been confirmed that feed-water oxygenation treatment for supercritical units can inhibit the flow-accelerated corrosion of the steels in high temperature water[6], but it was seldom reported about the oxygenation treatment on the oxidation properties of the superheater and reheater materials in the ultra-supercritical vapor. Some literatures revealed that oxygen from oxygenation treatment was attributed to the inhibition of the steel oxidation. Different dissolved oxygen concentrations on the oxidation properties of P91 steels has been studied by Chen at the supercritical vapor[7] and the oxidation films of P91 were of two layer structures with the outer of the iron oxide scale and the inner

Received date: December 25, 2017
Foundation item: National Natural Science Foundation of China (51371132)
Corresponding author: Yao Yuhong, Ph. D., Associate Professor, Shaanxi Provincial Key Laboratory of Photoelectric Functional Materials and Devices, Xi'an Technological University, Xi'an 710021, P. R. China, Tel: 0086-29-86173324, E-mail: yyhong0612@xatu.edu.cn

of the iron chromium oxide. But in high dissolved oxygen concentration, the outer layer were much thicker, the oxide particles were extremely finer and more holes were between the inner and the outer oxidation films which resulted in the worse cohesion with P91 matrix. It was also reported by Ehlers et al that the constant of oxidation rate of P91 was affected by the formation rate of $Fe(OH)_2$ controlled by dissolved oxygen concentration[8]. The high dissolved oxygen concentration could cause greater mass gain of HT9 steels at 500 °C water vapor, which was confirmed by Ren[9]. Zhang also reported that the oxidation mass gain of P92 steels in supercritical vapor at 550 °C increased with the increase of dissolved oxygen concentrations[10]. Detail researches were conducted by Ampornrat for T91, HCM12A and HT9 steels in the water vapor with different dissolved oxygen concentrations of 25, 100, 300 and 2000 μg/L and the mass gain in 2000 μg/L was the biggest, while it in 300 μg/L was the smallest which is very close to that in 100 μg/L[11]. In the present paper, the high temperature vapor oxidation tests were conducted on GH2984 in different dissolved oxygen concentrations and the effects of the dissolved oxygen concentration on the oxidation behavior were discussed.

1 Experiment

GH2984 alloy was used for the experiment with the standard heat treatment parameters of 1100 °C/1 h/AC+760 °C/8 h/FC~650 °C/16 h/AC. Its chemical composition is listed in Table 1. The samples with the size of 15 mm×10 mm×2 mm were first prepared by wire-electrode cutting. Secondly, for easy to be hanged up, the hole with the nominal diameter of 2 mm was drilled on the top end. Thirdly, careful mechanical polishing procedure using the waterproof abrasive paper numbered 280#, 400#, 800# and 1200# in turn was conducted to obtain the specimen surface characterized by no thick scratches, smoothness and uniform roughness. Finally, the specimens were cleaned by the alcohol and dried by the warm air. The microstructure of the specimen presented in Fig.1 is mainly austenite with the gain size of 70 μm and the twins in some grains, which are etched in

Table 1 Chemical composition of GH2984 alloy (wt%)

Cr	Si	Mn	Nb	Mo	Ti	Al	Fe	Ni
18~20	≤0.5	≤0.5	0.9~1.2	1.8~2.2	0.9~1.2	0.2~0.5	32~34	Bal.

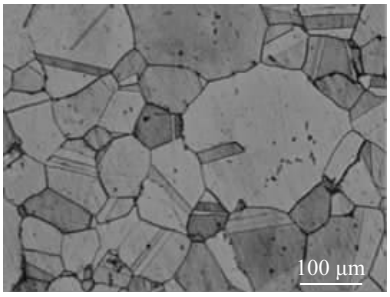

Fig.1 Microstructure of GH2984 alloy

5 g $FeCl_3$+25 mL HCl+25 mL H_2O solution.

Saturated steam oxidation tests with different dissolved oxygen concentrations of 10 μg/L and 5 mg/L were conducted on the device in Fig.2. Ultrapure water with the resistivity of 18.25 MΩ·cm (the dissolved oxygen concentration is about 5 mg/L) was intensively mixed with nitrogen in the multi-chamber deaerator to decrease the dissolved oxygen concentration to 10 μg/L. Before the saturated steam oxidation test, the ultrapure water with the dissolved oxygen concentration of 10 μg/L or 5 mg/L was preheated to 220 °C in the furnace (see Fig.2) to make the continuous flow steam into the reactor with the temperature of 300 °C and when the water vapor became saturated, the reactor was allowed up to the experiment temperature. The steam parameters of the reactor are the experimental temperature of 750 °C, the pressure of 0.1 MPa and the steam flow of 100~120 mL/s. The specimens were oxidized in the reactor for 50, 100, 200, 300, 500, 700 and 1000 h. At the end of the experiment, the steam was held into the reactor until its temperature was lower than 300 °C. The weight of the specimen was measured by the electronic balance with the precision of 10^{-2} mg before and after different oxidation time. The surface and cross section morphologies as long as the element distribution of the oxidation layer were observed by scanning electron microscope (SEM) with energy dispersive X-ray spectroscopy (EDS) (Hitachi-S4800). The phase structures of the oxidation layer were analyzed by X-ray diffractometer (Shimazdu-7000SX-XRD) and for the oxide integrity the electroless nickel plating process was employed on the pre-embedded specimens.

2 Results

2.1 Oxidation kinetics

Fig.3 shows the oxidation kinetics curves and fitting relationship between the square of mass gain and oxidation time of GH2984 alloy oxidized for 1000 h in 750 °C water vapor with different dissolved oxygen concentrations. It can be seen from Fig.3a that the curves in different dissolved oxygen concentrations are basically parabola, but the oxidation mass gain for 1000 h increased from 0.28 $mg\cdot cm^{-2}$ to 0.40 $mg\cdot cm^{-2}$ with the increment of the dissolved oxygen concentration from 10 μg/L to 5 mg/L. It is also seen from Fig.3a that the oxidation rates in different dissolved oxygen concentrations decrease when the oxidation time is longer than 50 h.

According to fitting relationship between the square of mass gain and oxidation time of GH2984 alloy in Fig.3b, the square of mass gain is approximately linear to the oxidation time which is described by Eqs. (1) and (2).

$$y = -0.00186+8.039\times10^{-5}x \quad (R^2=0.97) \quad (1)$$

$$y = -0.00342+1.617\times10^{-4}x \quad (R^2=0.98) \quad (2)$$

It is shown that the oxidation rate constant in the dissolved oxygen concentrations of 10 μg/L and 5 mg/L was 8.039×10^{-5} and 1.617×10^{-4} $mg^2\cdot cm^{-4}\cdot h^{-1}$, respectively.

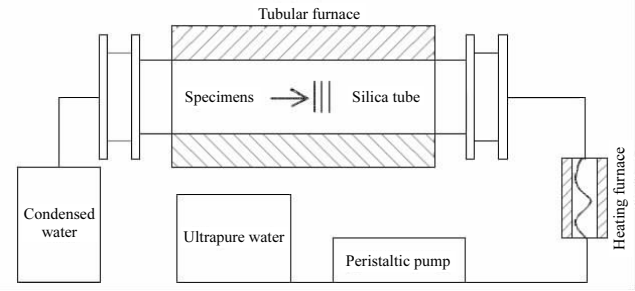

Fig.2 Schematic diagram of steam oxidation apparatus

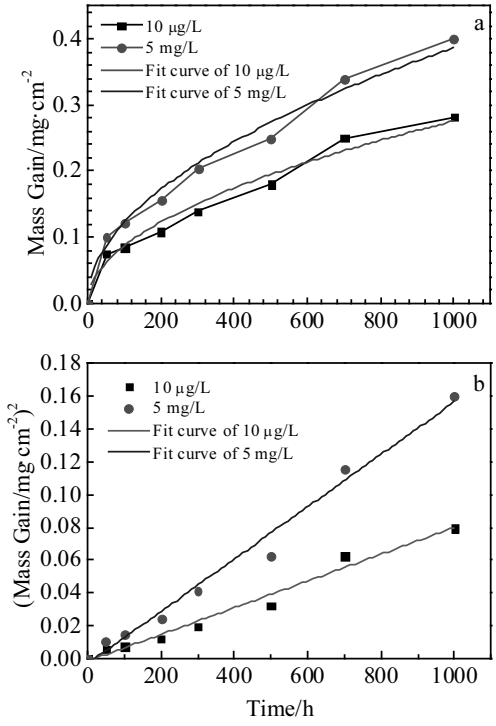

Fig.3 Oxidation kinetics curves (a) and fitting relationship between the square of mass gain and oxidation time (b) of GH2984 alloy oxidized for 1000 h in 750 °C water vapor with different dissolved oxygen concentrations

2.2 Composition and morphology in the surface of the oxidation film

Fig.4 is XRD patterns of GH2984 alloy oxidized for 1000 h in 750 °C water vapor with the dissolved oxygen concentrations of 10 μg/L and 5 mg/L. The characteristic diffraction peaks of both Cr_2O_3 and TiO_2 were observed in the XRD patterns and the peak intensity of Cr_2O_3 was apparently higher than that of TiO_2, which reveals that the main composition of the oxidation film in different dissolved oxygen concentrations is Cr_2O_3.

Fig.5 shows the surface morphologies of GH2984 alloys oxidized for 1000 h in 750 °C water vapor with the dissolved oxygen concentration of 5 mg/L and 10 μg/L. From Fig.5a, it

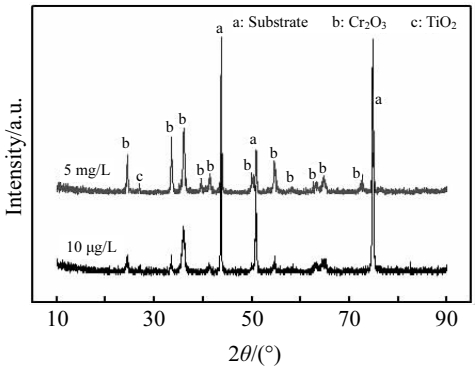

Fig.4 XRD patterns of the surface of the oxidation film in GH2984 alloy oxidized for 1000 h in 750 °C water vapor with the dissolved oxygen concentration of 10 μg/L and 5 mg/L

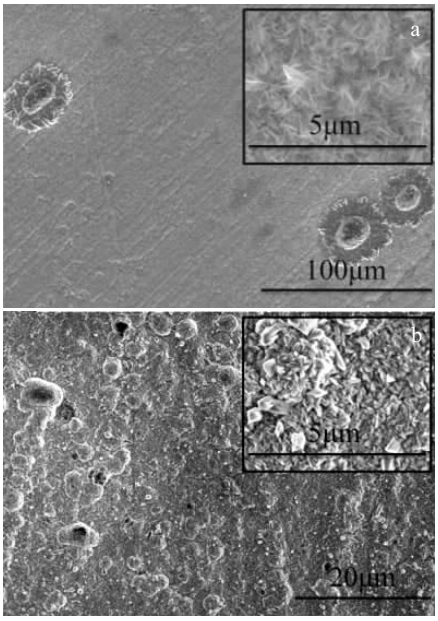

Fig.5 Surface morphologies of GH2984 alloy oxidized for 1000 h in 750 °C water vapor with different dissolved oxygen concentrations: (a) 10 μg/L and (b) 5 mg/L

could be seen that there is mainly needle-like oxide of Cr-rich on the surface of the sample oxidized for 1000 h at low oxygen pressure and the hand polished scratches on the surface were observed under the thin oxide film. It was reported that chromium and chromia-forming alloys could grow oxide whiskers or needles under atmospheres with low oxygen partial pressure and some water vapor content and the continued growth of a needle was sustained by rapid diffusion of metals along a dislocation or bundle of parallel dislocations. So it was clear that the growth of Cr_2O_3 needles would indicate very rapid transport of chromium from GH2984 alloys through the oxide. Moreover, it is noted that some

flower like oxides of Fe-rich in size of about 50 μm are distributed on the Cr-rich oxide film, and EDS analysis shows that the oxides of Fe-rich are composed of 50 wt% Fe, 30 wt% O, 14 wt% Cr and 6 wt% Ni. Fig.5b shows that the surface is covered with the light-grey wart like Cr-rich oxide particles. Previous researches[12,13] have investigated the oxidation behavior of GH2984 alloys in pure steam with the dissolved oxygen concentration of 5 mg/L oxidized at 750 °C for 100, 200, 500 and 1000 h and found that because of the short-cut diffusion of Cr throng the oxide, the spiculate Cr_2O_3 forms on the surface of GH2984 alloys for 100 h and with increasing of the oxidation time, the rapid diffusion channels are blocked in the spiculate Cr_2O_3 and it gradually changes to the granular oxide. So from the close-up view on the upper right in Fig.5, it could be inferred that the spiculate Cr-rich oxide became granular with increasing of the dissolved oxygen concentration.

2.3 Cross section morphology of the oxide film

Cross section morphologies of GH2984 alloy for 1000 h in 750 °C water vapor with the dissolved oxygen concentration of 5 mg/L and 10 μg/L are presented in Fig.6. It can be easily seen from Fig.6 and Fig.7 that a smooth, continuous and dense Cr-rich oxide film forms in the initial surface of the specimen surface, regardless of the dissolved oxygen concentration.

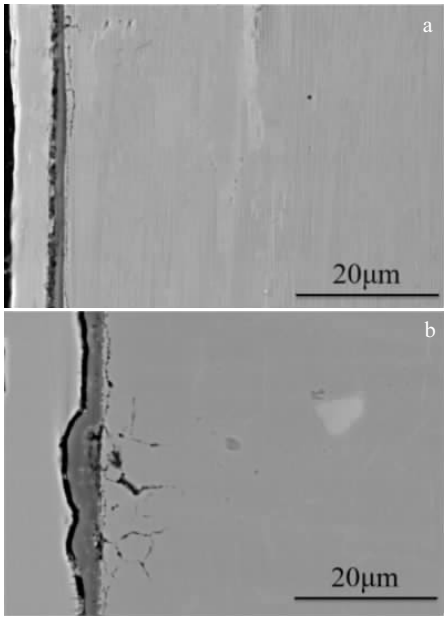

Fig.6 Cross-section morphologies of GH2984 alloy oxidized for 1000 h in 750 °C water vapor with different dissolved oxygen concentrations: (a) 10 μg/L and (b) 5 mg/L

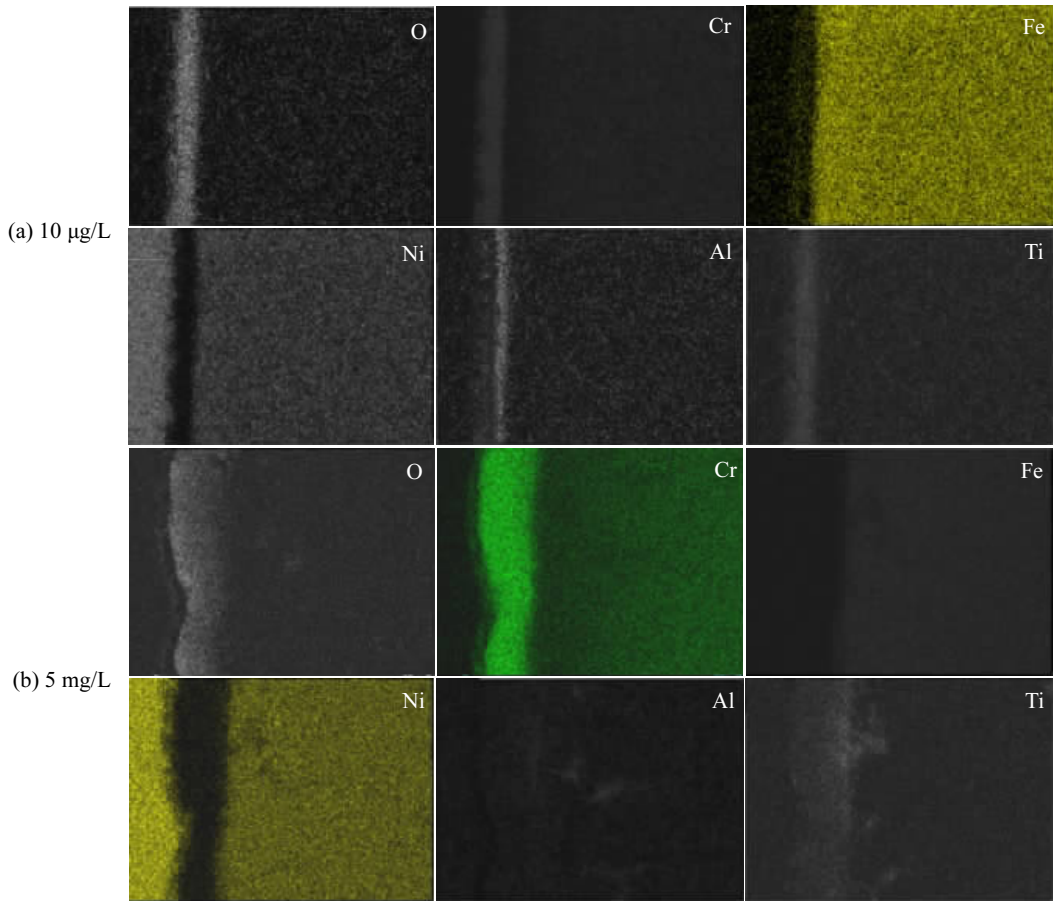

Fig.7 Cross-section element distribution of GH2984 alloy oxidized for 1000 h in 750 °C water vapor with different dissolved oxygen concentrations: (a)10 μg/L and (b) 5 mg/L

However, the thickness of the oxide film in the dissolved oxygen concentration of 5 mg/L is higher than that in the dissolved oxygen concentration of 10 μg/L. For the former, the serious internal oxidation and some Al-rich and Ti-rich oxides were observed in the oxidation film (see Fig.7b). As for the latter, Cr depletion zone with depth of 3 μm in the matrix under oxidation film rather than internal oxidation was seen in the film (Fig.7a).

3 Analysis and Discussions

Despite of the high content of Fe and Ni element in GH2984 alloys, Cr_2O_3 layer preferentially forms on the surface of the sample for the faster selective oxidation rate of Cr than that of Fe and Ni, which prevents the diffusion of Fe and Ni element and the generation of Ni, Fe oxides. Even though the spiculate Fe_2O_3 forms in the initial stage, it would be reduced and the generated O reacts with Cr to produce Cr_2O_3 with the increasing of the oxidation time for the more chemical activation of Cr.

For the formation of the stable Cr_2O_3 film by the reaction between Cr and the water vapor, Cr is one of the important elements to the steam oxidation resistance of GH2984 alloy. But at the high temperature Cr_2O_3 can react with O_2 or H_2O and O_2 to form the volatile CrO_3 [14] and $CrO_2(OH)_2$[15], respectively. Thus, the dissolved oxygen content in the steam will directly influence the stability of Cr_2O_3 film and consequently influence the steam oxidation resistance of GH2984 alloy. There are no obvious cracks and volatile CrO_3 or $CrO_2(OH)_2$ in Cr_2O_3 film of GH2984 alloy oxidized for 1000 h in 750 °C water vapor with different dissolved oxygen concentrations of 10 μg/L and 5 mg/L, which reveals that there is no effect of oxygenated treatment on the compactness of the oxidation film and the volatile rate of Cr element. But for the low dissolved oxygen concentration, a small quantity of flower-like Fe_2O_3 forms by the steam passing through thin Cr_2O_3 film (Fig.5a)[9]. For more oxygen molecules per unit time gathering on the surface of the sample in high dissolved oxygen concentration of 5 mg/L, the initial oxidation rate of GH2984 alloy is faster and the internal oxidation is obvious. It is well known that the diffusion speed of Al and Ti is higher than that of Cr in GH2984 alloys and both Al and Ti have a high solubility in Cr_2O_3[12,13]. Moreover, TiO_2 and Al_2O_3 are more stable than Cr_2O_3 and easily dissolved in Cr_2O_3 film. When Cr_2O_3 film grows to a steady stage, the internal oxides of Al_2O_3 and TiO_2 preferentially form in the grain boundary by the low content of Al and Ti in GH2984 alloy combined with oxygen passing through Cr_2O_3 film (Fig.7b).

4 Conclusions

1) The oxidation kinetics curves of GH2984 alloy oxidized for 1000 h in 750 °C water vapor with different dissolved oxygen concentrations (10 μg/L, 5 mg/L) are basically parabola, and the oxidation rate constants in the dissolved oxygen concentrations of 10 μg/L and 5 mg/L are 8.039×10^{-5} and 1.617×10^{-4} $mg^2\cdot cm^{-4}\cdot h^{-1}$, respectively.

2) The single oxide layer of GH2984 alloy oxidized for 1000 h in 750 °C water vapor with different dissolved oxygen concentrations (10 μg/L, 5 mg/L) is mainly composed of continuous Cr_2O_3 and a small amount of TiO_2. Moreover, the dispersive or local clustered internal oxides of Al_2O_3 and TiO_2 are observed in oxide layer with dissolved oxygen concentrations of 5 mg/L.

3) Oxygenated treatment causes the oxidation mass gain of GH2984 alloy to slightly increase, the internal oxidation to become more obvious, the thickness of the oxide film to enhance, a small amount of flower-like Fe_2O_3 to disappear and large quantity of the wart like Cr-rich oxides to form.

References

1 Bugge J, Kjaer S, Blum R. *Energy*[J], 2006, 31(10-11): 1437

2 Viswanathan R, Henry J F, Tanzosh J *et al*. *Journal of Materials Engineering and Performance*[J], 2005, 14(3): 281

3 Fukuda M, Saito E, Tanaka Y *et al*. *Proceedings of 6th International Conference Advances in Materials Technology for Fossil Power Plants*[C]. Santa Fe: ASM International, 2011: 325

4 Marion J, Drenik O, Frappart C *et al*. *Proceedings of IEA Clean Coal Centre Workshop: Advanced Ultrasupercritical Coal-fired Power Plants*[C]. Vienna: IEA, 2012: 4

5 Guo J T, Du X K. *Acta Metallurgica Sinica*[J], 2005, 41(11): 1221 (in Chinese)

6 Dooley R B. *Cycle Chemistry Guidelines for Fossil Plants: Oxygenated Treatment*[R]. Palo Alto, California: Electric Power Research Institute, 2005

7 Chen Y, Sridharan K, Allen T. *Corrosion Science*[J], 2006, 48(9): 2843

8 Ehlers J, Young D J, Smaardijk E J *et al*. *Corrosion Science*[J], 2006, 48(11): 3428

9 Ren X, Sridharan K, Allen T R. *Journal of Nuclear Materials*[J], 2006, 358(2-3): 227

10 Zhang N Q, Xu H, Li B R *et al*. *Corrosion Science*[J], 2012, 56: 123

11 Ampornrat P, Was G S. *Journal of Nuclear Materials*[J], 2007, 371(1-3): 1

12 Yang Z, Lu J T, Zhang X N *et al*. *Journal of Materials Engineering*[J], 2018, 46(1): 74

13 Yang Z, Lu J T, Gu Y F. *Rare Metal Materials and Engineering*[J], 2017, 46(4): 1013 (in Chinese)

14 Opila E J. *Materials Science Forum*[J], 2004, 461-464: 765

15 Opila E J, Myers D L, Jacobson N S *et al*. *The Journal of Physical Chemistry A*[J], 2007, 111(10): 1971

加氧处理对 700 ℃级超超临界锅炉合金 GH2984 饱和蒸汽氧化行为的影响

王　毓[1]，刘江南[1]，王正品[1]，要玉宏[1]，于在松[2]，鲁金涛[2]

(1. 西安工业大学，陕西 西安 710021)

(2. 西安热工研究院有限公司，陕西 西安 710032)

摘　要：采用氧化增重法、X 射线衍射、扫描电子显微镜研究了不同溶解氧浓度下 700 ℃级超超临界锅炉用 GH2984 镍基合金的 750 ℃饱和蒸汽氧化行为，结果表明： GH2984 合金在不同溶解氧浓度（10 μg/L、5 mg/L）的水蒸汽中生成的氧化层均为单层结构，主要由连续 Cr_2O_3 组成。加氧处理会造成 GH2984 合金氧化膜厚度增加和内氧化现象明显，并使得表面零散分布的 Fe_2O_3 瘤状凸起消失，转而生成更多富 Cr 瘤状凸起。另外，水中溶解氧浓度上升未引起 GH2984 合金表面 Cr_2O_3 氧化膜的加速挥发，但促进了 Cr_2O_3 氧化膜中少量 Al_2O_3 和 TiO_2 内氧化物的形成。

关键词：GH2984 镍基合金；蒸汽氧化；加氧处理；氧化膜

作者简介：王　毓，女，1982 年生，博士生，西安工业大学陕西省光电功能与器件重点实验室，陕西 西安 710021，电话：029-86173324，E-mail: rnawy@163.com